geologica**acta**

# Architectural characterization of a delta-front reservoir analogue combining Ground Penetrating Radar and Electrical Resistivity Tomography: Roda Sandstone (Lower Eocene, Graus-Tremp basin, Spain)

**M. COLL** [1,2]   **M. LÓPEZ-BLANCO** [1,3]   **P. QUERALT** [1,2]   **J. LEDO** [1,2]   **A. MARCUELLO** [1,2]

[1] **Institut de Recerca GEOMODELS – Group of Geodynamics and Basin Analysis, Facultat de Geologia, Universitat de Barcelona (UB)**
C/Martí i Franqués s/n, 08028 Barcelona, Spain.   Coll E-mail: miquelcoll@gmail.com

[2] **Departament de Geodinàmica i Geofísica, Facultat de Geologia, Universitat de Barcelona (UB)**
C/Martí i Franquès s/n, 08028 Barcelona, Spain.   Queralt E-mail: pilar.queralt@ub.edu

[3] **Departament d'Estratigrafia, Paleontologia i Geociències Marines, Facultat de Geologia, Universitat de Barcelona (UB)**
C/Martí i Franquès s/n, 08028 Barcelona, Spain.   E-mail: m.lopezblanco@ub.edu

─┤ A B S T R A C T ├─

Three-dimensional reconstruction of reservoir analogues can be improved combining data from different geophysical methods. Ground Penetrating Radar (GPR) and Electrical Resistivity Tomography (ERT) data are valuable tools, since they provide subsurface information from internal architecture and facies distribution of sedimentary rock bodies, enabling the upgrading of depositional models and heterogeneity reconstruction. The Lower Eocene Roda Sandstone is a well-known deltaic complex widely studied as a reservoir analogue that displays a series of sandstone wedges with a general NE to SW progradational trend. To provide a better understanding of internal heterogeneity of a 10m-thick progradational delta-front sandstone unit, 3D GPR data were acquired. In addition, common midpoints (CMP) to measure the sandstone subsoil velocity, test profiles with different frequency antennas (25, 50 and 100MHz) and topographic data for subsequent correction in the geophysical data were also obtained. Three ERT profiles were also acquired to further constrain GPR analysis. These geophysical results illustrate the geometry of reservoir analogue heterogeneities both depositional and diagenetic in nature, improving and complementing previous outcrop-derived data. GPR interpretation using radar stratigraphy principles and attributes analysis provided: 1) tridimensional geometry of major stratigraphic surfaces that define four units in the GPR Prism, 2) image the internal architecture of the units and their statistical study of azimuth and dips, useful for a quick determination of paleocurrent directions. These results were used to define the depositional architecture of the progradational sandbody that shows an arrangement in very-high-frequency sequences characterized by clockwise paleocurrent variations and decrease of the sedimentary flow, similar to those observed at a greater scale in the same system. This high-frequency sequential arrangement has been attributed to the autocyclic dynamics of a supply-dominated delta-front where fluvial and tidal currents are in competition. The resistivity models enhanced the viewing of reservoir quality associated with cement distribution caused by depositional and early diagenetic processes related to the development of transgressive and regressive systems tracts in high-frequency sequences.

KEYWORDS │ Reservoir analogue. GPR. ERT. Delta sandstones. Eocene. South-Pyrenean foreland basin.

## INTRODUCTION

Analyses of reservoir analogues in outcrop studies allow physical field observations that provide a crucial input to constrain similar reservoirs. These observations are widely used in resources estimation when direct subsurface measurements for oil or water reservoirs are limited. In order to consider a suitable reservoir analogue, several factors such as processes related to sedimentation, diagenesis and structural deformation should be regarded. Traditionally, the study of analogue deposits was carried out through sedimentological and structural analysis from outcrop data and sometimes with the complementary aid of well-logs. Nowadays, these studies can be improved with high resolution geophysical methods such as Ground Penetrating Radar (GPR) and Electrical Resistivity Tomography (ERT) surveys, which allow detailed 3D images of the subsurface. Interpretation of GPR and ERT, integrated with geological data from surface or well-logs, allow the reconstruction of a reliable Digital Solid Model to define the geometry and distribution of barriers and flow units (*e.g.* Corbeanu *et al.*, 2001; Pringle *et al.*, 2003). The Digital Solid Model is the integration of the surface and subsurface outcrop data in a Computer-aided design software (CAD), where the subsurface data are provided for geophysical methods and boreholes to complement the outcrop data called Digital Outcrop Model. Digital Solid Model (Pringle *et al.*, 2003) data

and the subsequent 3D architecture reconstruction allow a quantitative analysis of the spatial attributes to define the reservoir heterogeneity using various geostatistical tools to extract parameters for the geocellular modelling.

This methodology has been used for the detailed analysis of the internal architecture of one of the sandstone bodies from the Lower Eocene Roda Sandstone Formation, an Ypresian deltaic complex influenced by tides, located at the northern margin of the Graus-Tremp basin in Spain (Fig. 1). The aim of this study is to improve the knowledge about the sedimentary and diagenetic processes that produce heterogeneity in regressive bodies to complete the previous works on the Roda delta complex (Crumeyrolle *et al.*, 1991; López-Blanco, 1996; Marzo *et al.*, 1998; López-Blanco *et al.*, 2003; Tinterri, 2007). This reservoir analogue has well-exposed outcrops that allowed us to estimate the quality of the geophysical methods applied.

## GEOLOGICAL SETTING

The Pyrenees are an Alpine orogen with an E-W trend that was built from Late Cretaceous to Middle Miocene times due to the continental collision between the Iberian and Eurasian plates. The South-Pyrenean fold-and-thrust-belt contains an imbricated south-directed cover thrust system which consists, from north to south, in the Bòixols, Montsec and Serres Marginals thrust sheets (Fig. 1).
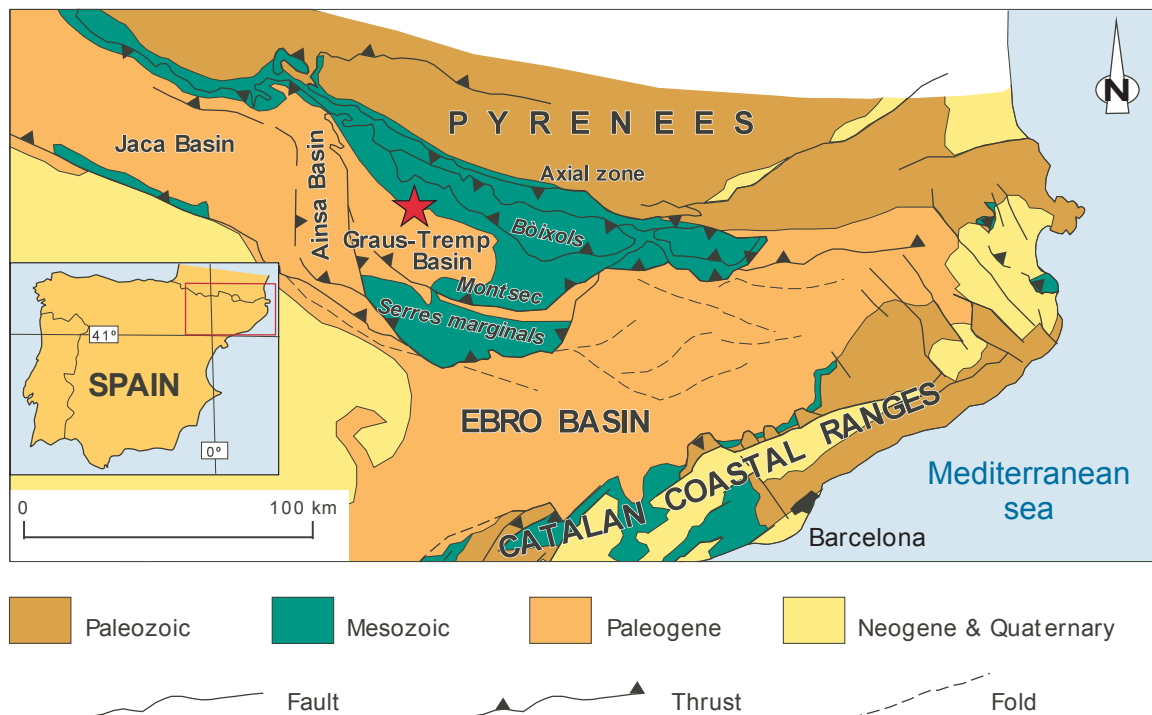


**FIGURE 1** | Geological location of the Roda Sandstone (star) on the central South-Pyrenean Zone.

These thrust sheets developed as part of a piggy-back thrust sequence during Late Cretaceous, Palaeocene-Early Eocene and Middle Eocene-Oligocene times, respectively (Muñoz, 1992, 2002; Meigs, 1997). The studied outcrop is located in the Graus-Tremp basin, a piggy-back basin developed on top of the Montsec thrust sheet during the Paleocene-Early Eocene, resulting from thrust propagation into the foreland.

The Lower Eocene Roda Sandstone belongs to the Paleogene infill of the Graus-Tremp basin. This stratigraphic unit has been subject of a great amount of geological studies (mostly sedimentological). Its depositional environment interpretation was originally attributed to littoral bars (Van Eden, 1970), to a sandwave complex (Nio, 1976) and to an Ebb-tidal delta (Yang and Nio, 1989). The last and more accepted environmental interpretation corresponds to a Gilbert-type delta system with tidal influence (Puigdefàbregas *et al.*, 1985; Tosquella, 1988; Crumeyrolle *et al.*, 1991; López-Blanco, 1996; Marzo *et al.*, 1998; López-Blanco *et al.*, 2003; Tinterri, 2007) that displays an overall regressive-transgressive trend. The Roda Sandstone interfingers and merges basinward into offshore calcareous mudstones. It was subdivided into six main sand wedges (U, V, W, X, Y and Z in Fig. 2) (Tosquella, 1988; López-Blanco, 1996) that were further subdivided into a number of minor-scale progradational sandstone units separated by transgressive, terrigeneous and/or carbonate-rich, deposits. The alternation of thin transgressive deposits and thick progradational sandstone units correspond to high-frequency transgressive-regressive sequences (Fundamental sequences from López-Blanco, 1996;

Marzo *et al.*, 1998 or elementary sequences from Tinterri, 2007). The minor-scale sandstone units characterize the regressive systems tract of these Fundamental sequences. Within the regressive deposits, four main facies assemblages have been differentiated (López-Blanco, 1996; Marzo *et al.*, 1998; López-Blanco *et al.*, 2003): alluvial/delta plain/bay, delta front, tidal-bars and prodelta-offshore (Fig. 2). Most of the volume of sandstones were deposited in delta-front and subtidal sandbar environments. The petrographic composition of the sandstones is dominantly arkosic (medium sand) and about 30% of the grains in the sandstones are carbonate, partly modified by diagenesis relatively shortly after deposition (Molenaar *et al.*, 1988).

## GEOLOGY OF THE DELTA-FRONT RESERVOIR ANALOGUE ($Z_4$ UNIT, RODA SANDSTONE)

In this work we study the internal heterogeneities of a small portion of the regressive systems tract of the minor-scale fundamental sequences belonging to one (unit $Z_4$ in López-Blanco, 1996; Marzo *et al.*, 1998; López-Blanco *et al.*, 2003) have been studied (Fig. 2). $Z_4$ is a sandbody about 10m thick, delimited at the bottom and top by carbonate-rich levels. Figure 3 shows an outcrop, located very close to the place where geophysical data were acquired, where a stratigraphic log has been measured (Fig. 4). The log shows the regressive systems tract (down) and the transgressive systems tract (up) of two consecutive fundamental sequences separated by a maximum regression surface signaling a change in depositional trend.
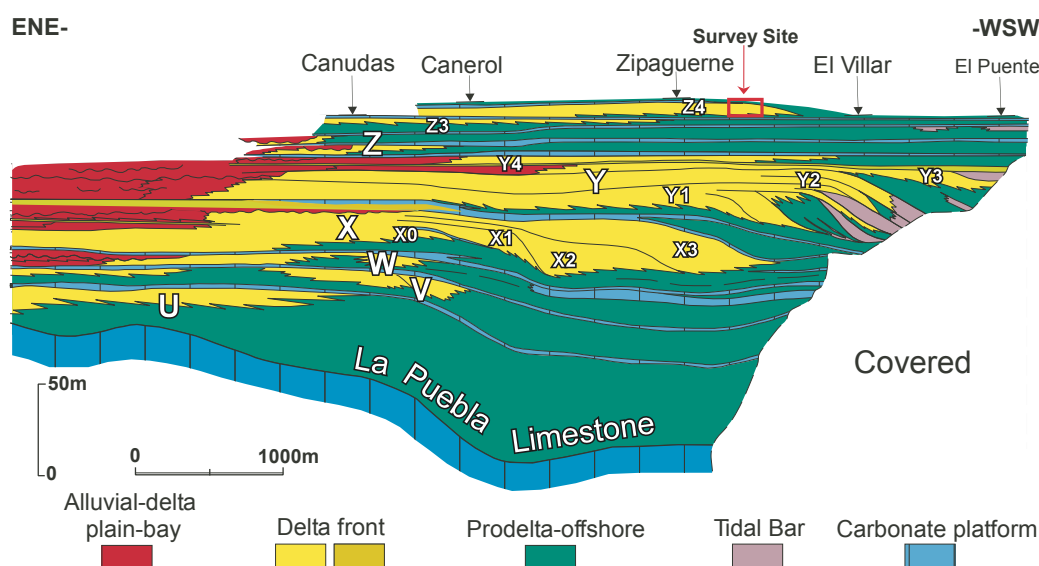


**FIGURE 2** | Outcrop-based geological cross-section of the Roda Sandstone Formation parallel to the main paleocurrent direction based on the correlation of 18 stratigraphic logs. Notice the vertical exaggeration. Six main sand wedges (U, V, W, X, Y, Z) interfinger and merge basinward into offshore mudstones. Sand wedges X, Y and Z, are subdivided into a number of subunits (X0-X3, Y1-Y3, Z0-Z4), (modified from López-Blanco et al., 2003).
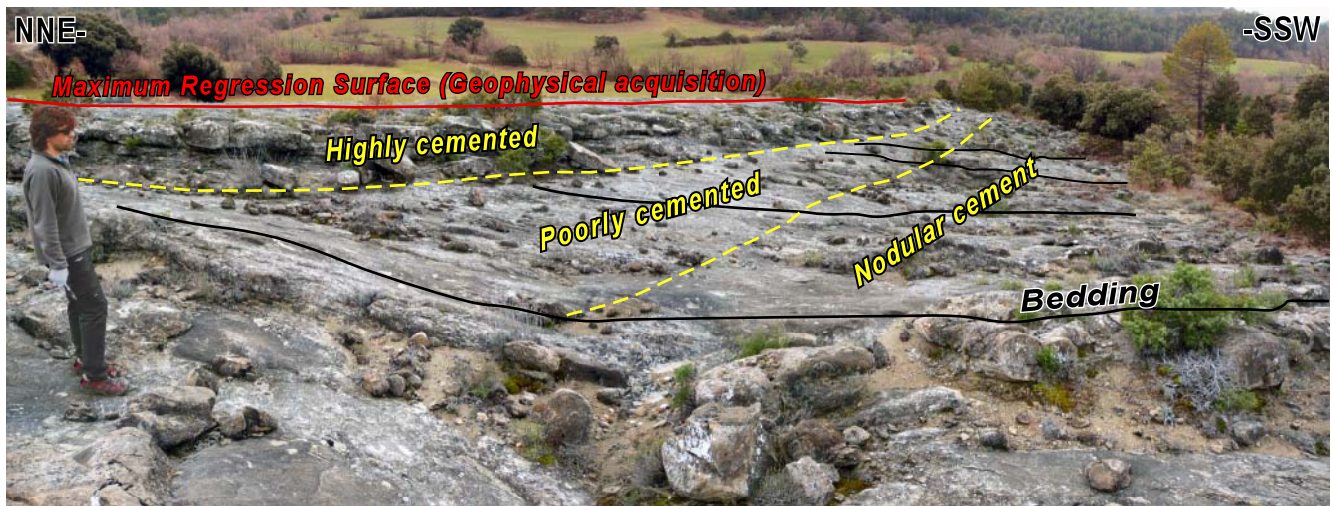
**FIGURE 3** | Outcrop view showing the concave-up SSW-dipping clinoforms of the $Z_4$ sandbody and their toplap/truncation relation with the upper maximum regression surface. Geophysical data were acquired on the maximum regression surface (red line). The yellow dashed lines delimitate different cementation zones in the sandstones. Black lines delineate some of the sandstone beds (megaforesets). Person for scale is approximately 1.76m tall.

The lower regressive systems tract (RST) is made by delta front sandstones showing metric to decametric concave-upwards megaforeset (metric-scale cross-stratification depositional surfaces) geometries moderately dipping SSW (dips up to 30º). These megaforesets occasionally show minor-scale (cm to dm scale) megaripple cross-bedding with an oblique to perpendicular orientation respect to the main foreset clinoforms. Those sandstones have been interpreted as prograding delta-front mouth-bar sandstones resulting from avalanche-processes operating in a Gilbert-type delta-front with slight tidal influence resulting in the oblique minor-scale cross bedding generated by ebb currents in a subtidal environment (López-Blanco, 1996; Marzo *et al.*, 1998; Tinterri, 2007). The internal stratification of the sandbody shows clinoforms with downlap geometry on top of a maximum flooding surface and a toplap (erosional truncation) associated with the terminal maximum regression surface (Fig. 3). The maximum regression surface is coincident with a marine ravinement surface where the upper part of the prograding delta lobe was eroded and transformed into a relatively regular and planar surface by wave action. The sand below this truncation surface is cemented to 0.5 meters below the surface and it is characterized by processes of bioturbation, infiltration and mixing of matrix, and precipitation of penecontemporaneous rim-cement generating a hardground, highly-cemented horizon (Molenaar *et al.*, 1988). This fact implies that this surface can be also considered as a marine flooding surface (transgressive surface) generated during transgression below main fair-weather wave base. Cement distribution is not homogeneus along the $Z_4$ sandbody. There is a lower part with concretionary (nodular) cementation, an intermediate poorly-cemented zone just below the mentioned upper hardground (Fig. 4).

Above this boundary (maximum regression surface), shallow water bioclastic sandstones, sandy limestones and offshore marls (Fig. 4) represent deposition on a shallow water mixed platform with minor detrital input during a transgressive episode (transgressive systems tract).

On the study oputcrop, most of the transgressive systems tract deposits have been removed by erosion allowing the exposure of a gently SE-dipping exposed platform of about 3000m² coincident with the maximum regression surface. Geophysical measures were carried out on this surface due to the fact that it displays a nearly flat platform with a constant topographic gradient which enables a better antenna-ground coupling and simplify processing steps like migration (Lehmann and Green, 2000).

## METHODS; GPR AND ERT DATA

GPR and ERT were chosen together to better characterize the physical and chemical composition of the subsurface, since the images obtained are response of different electrical proprieties as dielectric permittivity and electrical conductivity, respectively. The acquisition of shallow subsurface data was carried out on the $Z_4$ unit (Figs. 2 and 5). The GPR datasets acquired consist of test lines, common midpoint (CMP), and a dense grid of GPR traces producing a prism created by performing a linear interpolation between successive radargrams. These data have been complemented by three ERT profiles. Finally, a leveling survey with Total Station, Leica Tc 1700, provided topographic corrections and a reference datum for geophysical data sets.
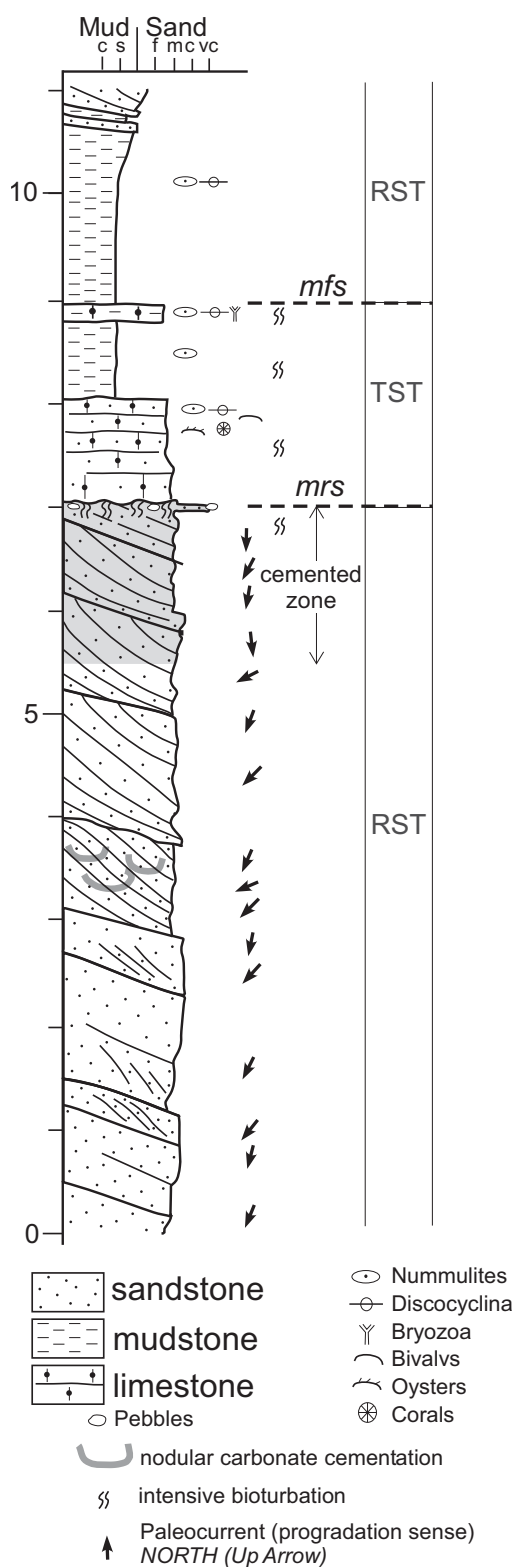
## Ground Penetrating Radar; data acquisition and processing

GPR is a geophysical method that transmits high frequency (12MHz-4500MHz) pulsed electromagnetic waves into the ground surface. The electromagnetic waves are reflected on the interfaces of changes in electrical properties, returning to the surface and intercepted by the receiver antenna. This method provides a high resolution image of the subsurface like the geometry of buried objects or geologic structures. The reflection coefficient describing the amplitude which is reflected from a certain interface is defined, mainly, by the dielectric permittivity (Davis and Annan, 1989). In the same way, the electrical conductivity of the rocks controls the penetration depth of electromagnetic waves, introducing absorptive losses. This loss is primarily dependent on the water content and mineralization present. Studies on dry reservoir analogues are favorable because lithological components (gravel, sand and carbonates) have low conductivities and, therefore, low attenuation. Many authors have demonstrated the value of GPR revealing in great detail the internal architecture of ancient and modern reservoirs of different depositional environments at the subseismic scale (*e.g.* Corbeanu *et al.*, 2001, 2004; Szerbiak *et al.*, 2001; Pringle *et al.*, 2003; Jol *et al.*, 2003). More precisely, some of these studies have been carried out in similar depositional environments to the one discussed in this paper (Lee *et al.*, 2005, 2007, 2009).

GPR data were acquired with a Pulse Ekko™ 100 system manufactured by Sensors and Software Inc. using antennas with center frequencies of 25, 50 and 100MHz. The data was collected with common offset profiles keeping a single transmitter and receiver with a fixed spacing between antennas, which is transported along a survey line to map reflections versus position. Those profiles were collected with 64 stacks for each trace to improve the signal-to-noise ratio and using a time window of 300ns. The antennas orientation was perpendicular to the direction of survey (perpendicular broadside).

Two preliminary test GPR lines were collected at 25, 50 and 100 MHz to determine optimal data acquisition parameters (Fig. 5B). These lines were acquired perpendicularly, one oriented parallel to the general dip direction of the delta-front clinoforms (line 1), whilst the other is oriented parallel to the strike direction (line 2). In addition, along line 1, four CMP were acquired using 100MHz antennas to extract the migration and replacement velocity.

After georeferencing the raw data, we proceeded to make a basic processing: aligning first arrivals, adjustment time-zero, dynamic correction (wave velocity=0.095m/ns), signal saturation correction (dewow), background removal,
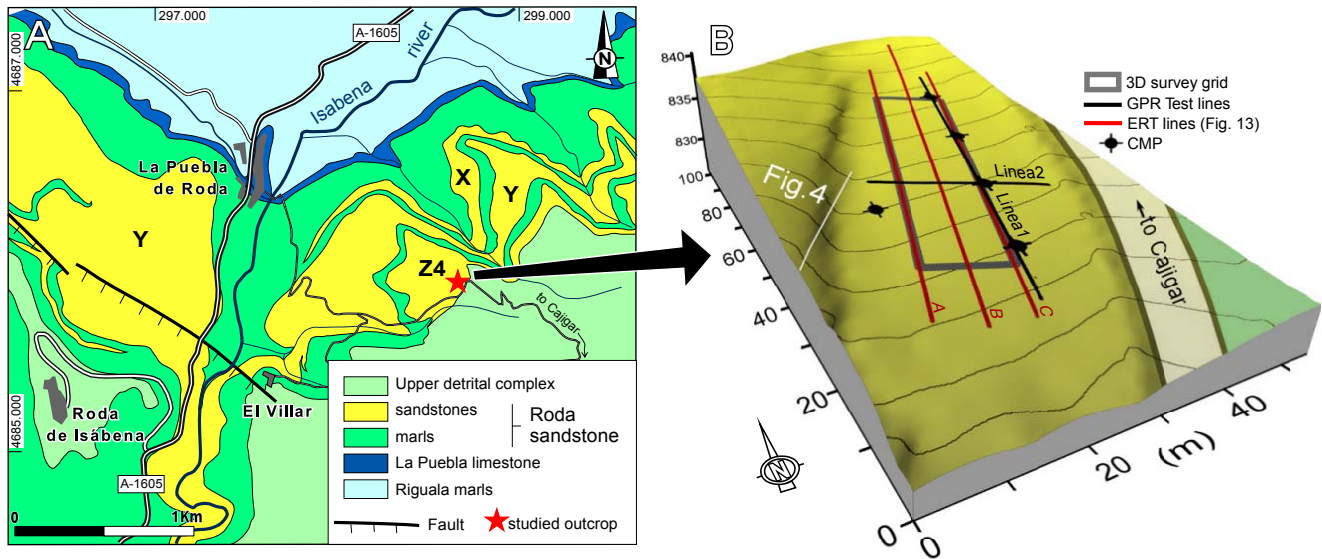
**FIGURE 5** | A) Geological map of the Roda Formation with the location of the studied outcrop and the main sandstone bodies. B) Digital Elevation Model of the studied outcrop with location of the GPR and the ERT surveys and the stratigraphic log (see Fig. 4). CMP indicate the center of Common-Midpoint profiles. Outcrop coordinates: 42º 17' 48"N, 33' 22"E.

bandpass filters are applied to improve the signal-to-noise ratio (the filter bandwidths chosen from the 25MHz, 50MHz and 100MHz were 0-75MHz, 0-110MHz and 0-250MHz respectively) and the gain (energy decay curve) in order to compensate the amplitude loss due to the geometric spreading and the soil attenuation. Subsoil propagation velocity of 0.095m/ns is obtained from four CMP surveys along line 1 using the 100MHz antenna to obtain better resolution. This velocity was used as input in the dynamic correction, 3D Kirchhoff migration and to convert two-way travel time to depth, the last two steps only have been process in the prism data. Finally, a topographic correction was applied.

Processed profiles collected along test line 1 with three different antennas are shown on Figure 6. All profiles show SE-inclined reflections interpreted as depositional surfaces depicting the megaforesets observed on the outcrop (Fig. 4). As expected when the profiles of Figure 6 are compared, a resolution increase along with antenna center frequencies is observed (Davis and Annan, 1989), identifying the reflectors with greater detail on profiles with 100MHz antenna. On the profiles in line 2 (Fig. 5), perpendicular to line 1, reflectors are sub-continuous and show low-angle apparent dips in both directions ESE and NNW.

To build a GPR prism, a 50MHz antenna was chosen as a compromise between resolution (~1m), depth of penetration and clutter limitations (Annan and Cosway, 1994). The accurate location of each trace is critical to produce a 3D display. Positioning errors result in a mis-reconstruction of the true geometry of the reflectors using

a 3D migration algorithm (Groenenboom *et al.*, 2001). For this reason, a precise grid was constructed on the outcrop surface. It consisted of 31 SSW-NNE in-lines spaced by 0.4m with a step size of 0.4m, therefore obtaining a regular grid of 12 per 48m. This grid spacing is less than a quarter wavelength of the center frequency (50MHz) to obtain unaliased recording of dipping reflections and diffractions (Grasmueck *et al.*, 2005).

**Electrical Resistivity Tomography; data acquisition and processing**

GPR data were complemented with electrical resistance tomography collected with an Syscal Pro (IRIS-Instruments company) with 72 electrodes. The method is based on the injection of an electric current by means of two electrodes and measuring the potential between two other electrodes (Ward, 1990). The apparent resistivity can be obtained from the measured values of the potential difference and current intensity. To construct a pseudosection several measures are acquired. The apparent resistivity values are obtained moving sideways the four electrodes and increasing the separation between the electrodes to increase depth of investigation. Nowadays, the equipments measure different combinations of electrodes using a multi-core cable with as many conductors as electrodes plugged into the ground.

Three ERT profiles were obtained using Wenner-Schlumberger, this array provides good depth sensitivity and good resolution of horizontal layers for high signal-to-noise ratios (Ward, 1990). Two of the profiles were located on the SSW-NNE oriented prism boundaries (Fig. 5B) and
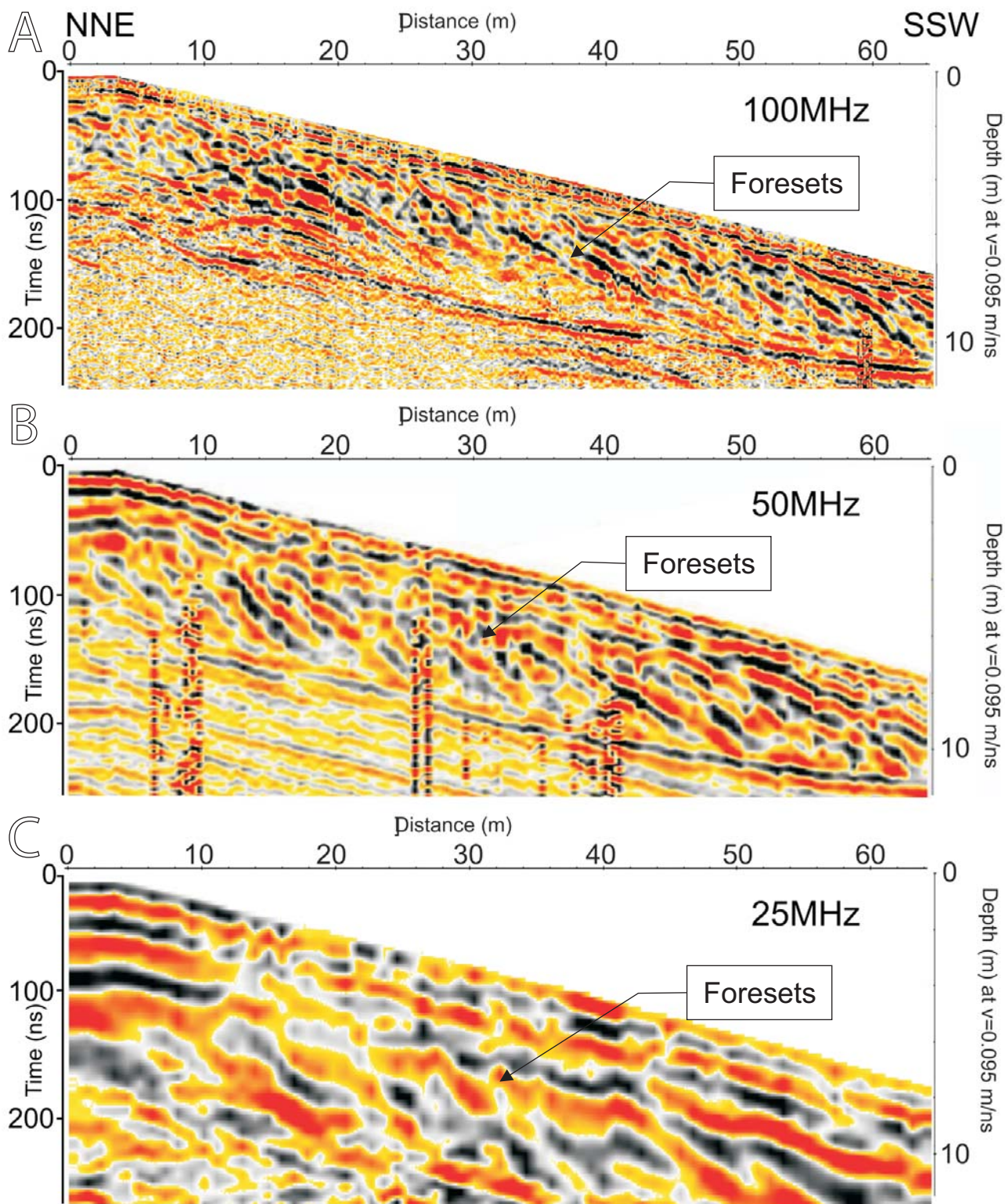
**FIGURE 6** | GPR profiles measured in test line 1 (see Fig. 5B), oriented parallel to mean foreset dip and measured with different antenna central frequency. A) 100MHz. B) 50MHz. C) 25MHz. These profiles show the inclined reflectors forestes with different resolution capturing the progradational character of the sandbody.

72 electrodes were spaced at 1m to enhance resolution. A third line located parallel and equidistant to the previous lines was obtained after the placement of 48 electrodes spaced at 2m intervals. This last line was acquired to better characterize the resistivity of the area and to extract information from deeper areas with the aim to imagine the bottom of the sandstone unit.

To obtain the true resistivity distribution in subsurface the apparent resistivity data were inverted using a program based on the smoothness-constrained least-squares method with a quasi-Newton optimization technique (Loke and Barker, 1996). The resistivity models obtained from the inversion have a root mean square (RMS) misfit of about 5%.

## INTERPRETATION AND RESULTS

After acquisition and processing, 3D GPR data were imported to seismic interpretation software to map depositional surfaces. The data analysis through geometric attributes may help to quantify and cottage the previous reflector interpretations.

The prism corresponding to the processed 3D GPR data analyzed is represented in Figure 7A.

The main results obtained from GPR and ERT data are: i) a tridimensional geometric control of individual depositional surfaces; ii) a statistical study of foreset dips (useful for determination of paleocurrent directions); iii) an image of the tridimensional internal architecture of the sandbody distinguishing different order surfaces and bedsets; and iv) the viewing of reservoir barriers associated with cement distribution.

## Stratigraphic analysis

To obtain a detailed internal architecture reconstruction of the sandbody, the reflection events were interpreted as mappable horizons. As a result, some horizons were reconstructed delineating the reflectors in each in-line section (oriented parallel to the acquisition direction) and cross-line sections (perpendicular to the acquisition direction). An example of one of these horizons interpolated from the delineation of 31 sections is shown in Figure 7B. Reconstructed surfaces show similar features, geometries and orientation to those observed in the nearby outcrop (Fig. 3) and also show nearly 1m thick megaforeset units similar to those observed in the stratigraphic log (Fig. 4). The reconstructed surfaces are curved and tangential to the base (concave-up), with a clear decrease of dips (from 18º to 4º) in a SSW direction. In a strike direction the reflectors do not exhibit major dip changes.

To understand internal sandbody architecture, radar stratigraphic analysis of the observed surfaces where a series of radar units were defined is presented. Radar stratigraphic analysis was developed in recent years (Gawthorpe *et al.*, 1993; Jol and Bristow, 2003), adapting
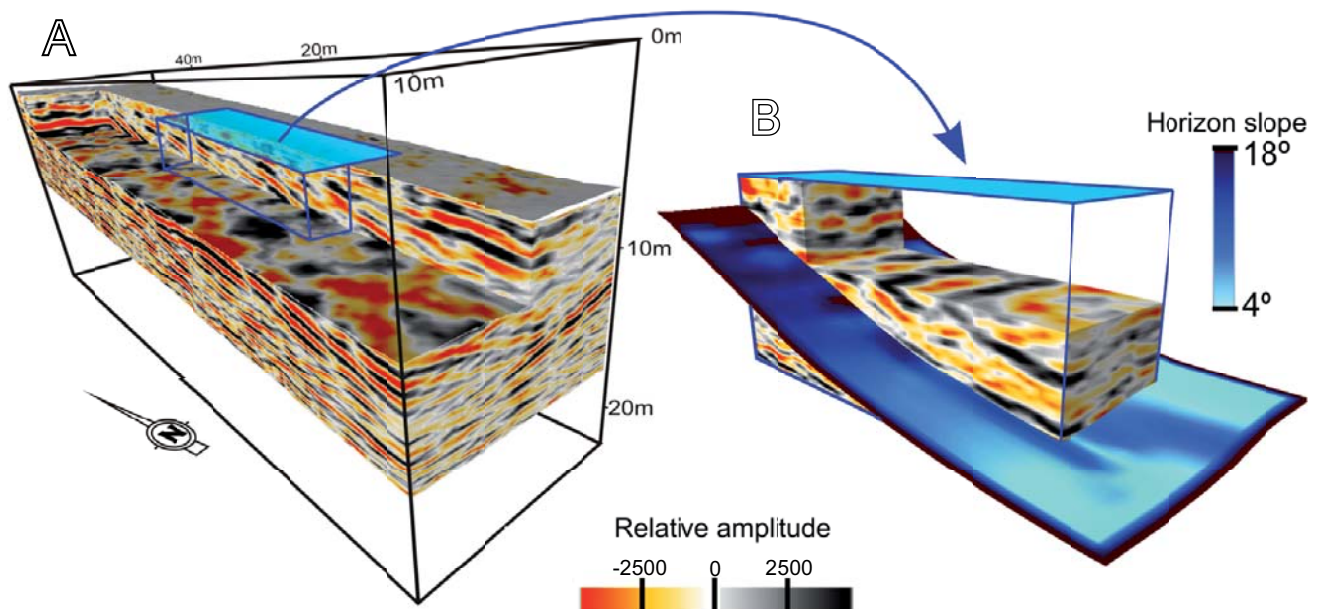


**FIGURE 7** A) Three-dimensional perspective view of the migrated GPR prism. The 50MHz data were collected in 12x48m grid with each line measured with a 0.4m step size, (see Fig. 5B). B) Example of a stratigraphic horizon resulting from 3D tracking.
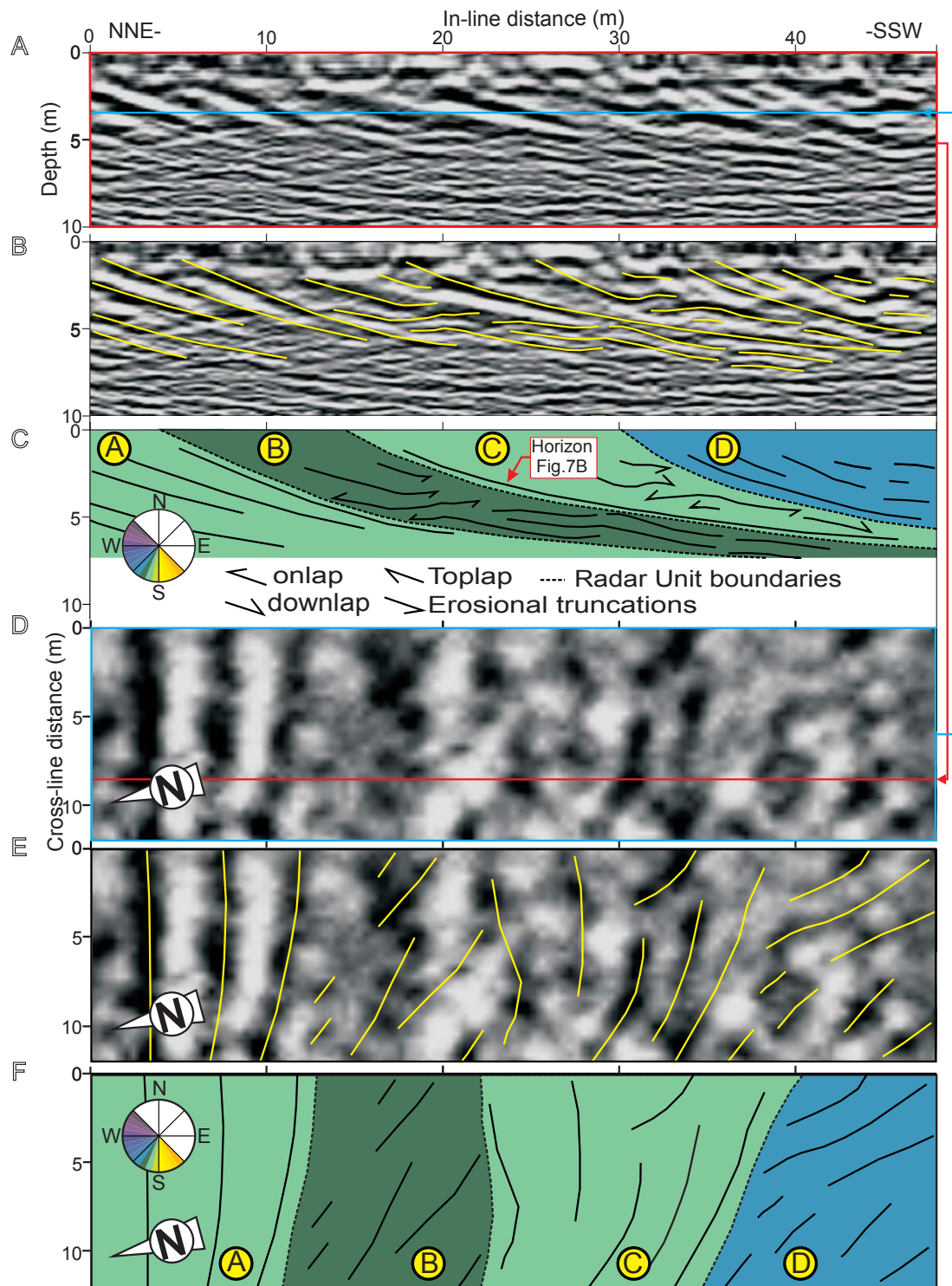
**FIGURE 8** | Representative vertical (A, B and C) and horizontal (D, E and F) sections across the 3D GPR prism including the data, line drawing of reflectors and stratigraphic interpretation. Notice that the horizontal section covers the whole extent of the GPR prism. A) Vertical section along the in-line situated at a cross-line distance of 8.8m (Blue line indicates the position where the In-line cross with the horitzontal section in Fig. 8D). B) Line-drawing of the reflectors. C) Stratigraphic interpretation of reflectors and sets subdivision. D) Horizontal section at 3.46m of the prism (red line indicates the position where the section crosses the vertical section in Fig. 8A). E) Line drawing of the reflectors. F) Stratigraphic interpretation of reflectors and sets subdivision. In C and F dash lines represent set boundaries and colors correspond to average paleocurrent direction for each set represented in the rose diagrams in C and F.

seismic stratigraphy principles (*e.g.* Mitchum *et al.*, 1977a, b; Brown and Fisher, 1980) to radar profiles and 3D prisms. The main characteristic features observed in the 3D data from $Z_4$ sandbody are illustrated through a vertical slice along the in-line and a time slice in Figure 8A, D. The maximum depth penetration is 7m, considering a homogeneous velocity of 0.095m/ns. Subsequent to line drawing (Fig. 8B, E), reflector terminations (*i.e.* where two reflectors converge to produce triple junctions).Were identified (Fig. 8C, F). The main types of reflector terminations observed are toplap or erosional truncation on the upper boundary of a radar unit and onlap or downlap on the lower boundary. These terminations must be interpreted carefully because these triple junctions can also result from interference patterns of coherent noise such as antenna ringing or air wave reflections. Furthermore, terminations can also be produced when the thickness of conformable strata decreases to values below the level of resolution, so-called apparent truncation (Gawthorpe *et al.*, 1993). Amplitude of the reflectors and their three-dimensional geometry provide assistance to identify the nature of these terminations.

After the identification of the stratigraphic terminations, these have been tracked systematically along the prism, obtaining three radar unit boundaries (thick lines on Fig. 8C, F and the surfaces on Fig. 9). Radar unit boundaries define genetically related packages of strata that are the fundamental stratigraphic units identifiable on GPR data (radar sequences in Gawthorpe *et al.*, 1993). This methodology allowed the definition of four radar units (A, B, C, D) reflecting different depositional events. These boundaries represent non-depositional (A-B and C-D) and erosional events (B-C) as deduced from the onlap and truncation geometries observed in Figure 8.

### Geometric attribute analysis

Since GPR data show the megaforeset surfaces in 3D (Figs. 6, 7, 8, 9) a paleocurrent analysis based on the clinoforms orientation has been made using dip direction as paleocurrent azimut. To determine the paleocurrent distribution, the spatial orientation of reflectors was measured using the Steering algorithm.

This algorithm is based on the 3D Fourier analysis technique (Tingdahl, 2003) and it works like a local autotracker that localizes the same event computing the similarity of adjacent trace segments. The dips of the
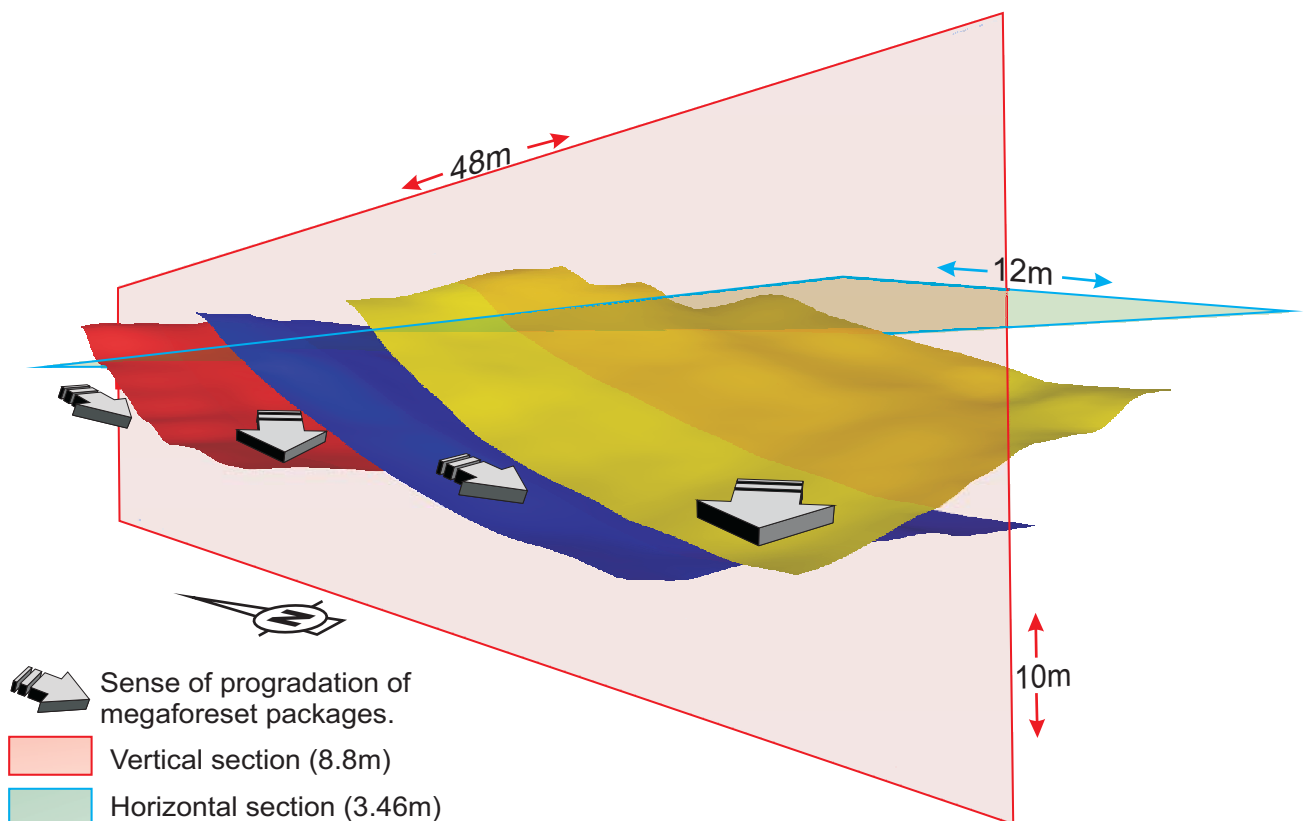


**FIGURE 9** | 3D expression of the radar unit boundaries extracted from GPR data. Notice the clockwise evolution of the dip. The arrows indicate the average dip of the four units calculated on geometric attributes. Red and Blue sections correspond to the sections shown in Figure 8.

events are stored in two components: in-line dip and cross-line dip; these storage values determine the steering prism. To determinate a correct dip analysis to understand paleocurrents the data have been updated to the original depositional position compensating the present day regional dip (170/7.5). A median filter was applied to obtain the more significant dips and to remove dips produced by random noise and local variation. After that azimuth and dip attribute were computed in each point of the steering prism. The azimuth values obtained were referenced to the North. Subsequently, the two attribute (dip and azimuth) in 1300 random positions were exported. These points were taken between 2 and 4.5 meters in depth, where the signal-to-noise ratio is better.

When compared the computed azimuth values (Fig. 10A) to the paleocurrent measured on the nearby outcrop in Figure 3 (Fig. 10B), the main dip direction (SSW) can be observed on both datasets. This fact reveals that GPR attributes are useful tools to obtain paleocurrent data and trends in this type of depositional setting.

Orientation values are represented by Azimuth/Dip graphics (Fig. 11) where absolute dip is correlatable to paleocurrent strength and azimuth to paleocurrent direction evolution linked to the defined sets and couplets. The data dispersion indicates a wider variability of azimuth values corresponding to lower dips. In Figure 11A, the color scale is a function of the distance to the northeastern border of the prism, corresponding to the more proximal area. In general, dips are higher to the northeastern part (where sediment comes from) and lower in more distal areas, signaling a progressive decrease in time of the strength of the currents that built the mouth bars.

Two dip-decreasing sequences: a first one from 0 to 24m (red and yellow colours) ranging progressively

from 20° to almost 3° and, after an abrupt increase of dip values, a second sequence from 24 to 45m (green and blue colours) ranging progressively from 14° to almost 3°.

The graph in Figure 11B was built taking into account the stratigraphic analysis done in the previous point. In this case, color scale represents the four distinguished radar units (sedimentary packages or depositional units) and two couplets (A+B and C+D). Each one of these couplets shows a decrease of the dip values and a clockwise variation of azimuth from 200 to 225 degrees and from 190 to 240 degrees respectively (Fig. 11). Azimuths associated with lowest dip values have not been taken into account because of their variability.
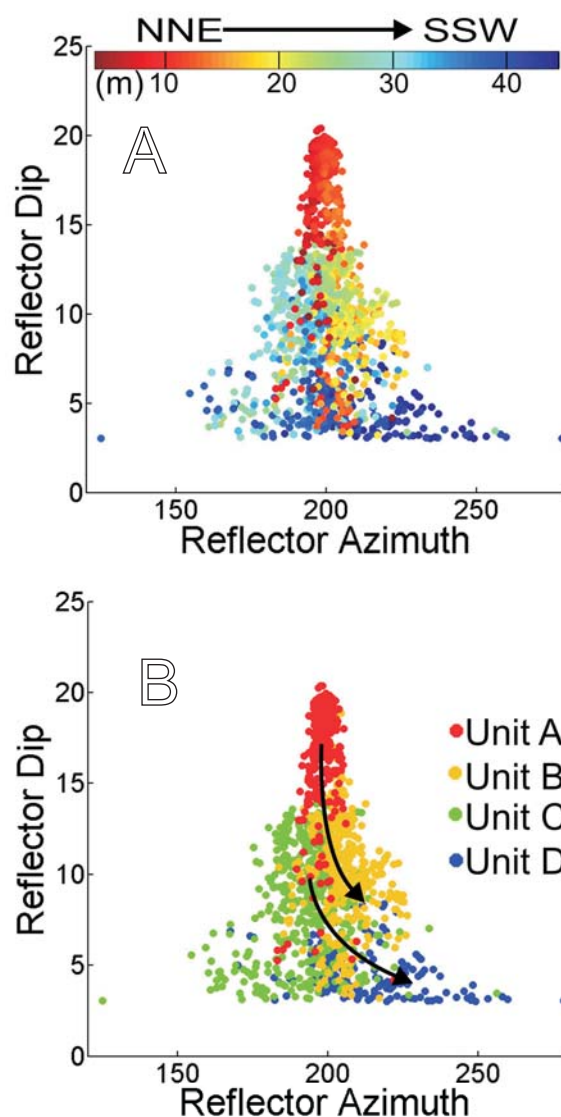


**FIGURE 11** | Azimuth/dip graphics. A) Distribution of the azimuth/dip data in relation to the distance from the north boundary of the prism. B) Distribution of the azimuth/dip in relation to the four sandstone sets defined in Figure 8 and delimited by the surfaces in Figure 9.



**FIGURE 10** | Rose diagram plots of: A) the reflectors dip direction calculated with the azimuth attribute in the GPR prism; B) the clinoforms dip directions measured with compass in the outcrop.

Combining paleocurrent data (Fig. 11) and internal architecture of the sandbody (Fig. 8), the sedimentary evolution of the delta-front can be deduced. Figures 8C, F show a composite sedimentary evolution of the delta-front where abandonment and erosive reactivation surfaces separate volumes of sandstone with different general paleocurrent trends. From Figure 8F we can determine two couplets of sandstone sets (as deduced in Fig. 11B). Both show a two-step period with the previously mentioned clockwise evolution of paleocurrents and a non-erosive bounding surface between sets (the boundary is almost parallel to stratification of the first set). The boundary between couplets is an erosional surface eroding the strata of the second set (Fig. 8).

After examining the set-bounding surfaces in 3D (Fig. 9), a similar general clockwise evolution of the dips of successive surfaces is observed. This evolution of the pro-gradational system corresponds to a section of less than 50m in dip direction and it matches with the observed in other outcrops of the Roda Sandstone (*eg.* X unit in Figs. 2, 12). The X sandbody shows a composite pattern made up by a series of small-scale sandbodies (10-20m thick and 200-700m long) separated by truncation and marine flooding surfaces. Most of the small-scale composite sandbodies show a clear clockwise paleocurrent evolution (as seen in the studied unit $Z_4$) and the X unit itself (30m thick and 1500-2000m long) also shows this evolution (from S-directed to WNW-directed paleocurrents). After the results obtained from GPR data interpretation it can be stated that the general clockwise paleocurrent evolution is an attribute present, at least at three different scales (kilometers, hundreds of meters and tens of meters), in the Roda delta complex.

It can also be observed that the variation on the paleocurrents decreases according to the size of the units. The paleocurrent variation in the whole X unit (1500 to 2000m long) is about 135°±45° whereas the rotation in the minor sandbodies within the same unit (200 to 700m long) are, on average, about 90°±45°. In the studied outcrop

the defined units are much smaller (10 to 20m long) and paleocurrent rotation show values much lower than those observed in larger-scale units, close to 20° on average.

## Resistivity distribution analysis

ERT data is proved here as a valuable tool to understand cementation distribution within the studied sandbody. Resistivity distribution in three pseudo-sections in acquisition direction of the GPR prism is shown in Figure 13. All three pseudo-sections show a similar pattern, characterized by a series of horizons parallel to the top of the sandstone unit. Four resistivity units can be distinguished (Fig. 13): i) a relatively high resistivity horizon at the top (0-1.75m); ii) a relatively low resistivity level (1.75-4m); iii) an intermediate-high resistivity zone (4-12m); and iv) a very low resistivity (below 12m).

Given the fact that the studied sandstone package shows a homogeneous lithology and grain size (Fig. 4), the different resistivity boundaries observed in ERT profiles could be caused by differential cementation of the sandstones observed in the outcrop (Figs. 3, 4). Comparison between the ERT pseudo-sections and the outcrop-derived data show a clear correlation. The uppermost resistive unit (0-1.75m) directly corresponds to the highly cemented horizon on top of the $Z_4$ sandbody, just below the maximum regression surface (Figs. 3, 4). This level has high values of resistivity, in response to the strong cementation below the major abandonment surfaces. The second, low resistivity layer (1.75-4m) corresponds to a poorly cemented horizon observed in Figures 3 and 4.

The third intermediate-high resistivity zone represents the lower half of the sandbody where concretionary calcite cementation occurs as non-coalesced concretions (lower nodulized area in Fig. 3). The lowermost, very low-resistivity unit is located between 10 and 15m below the
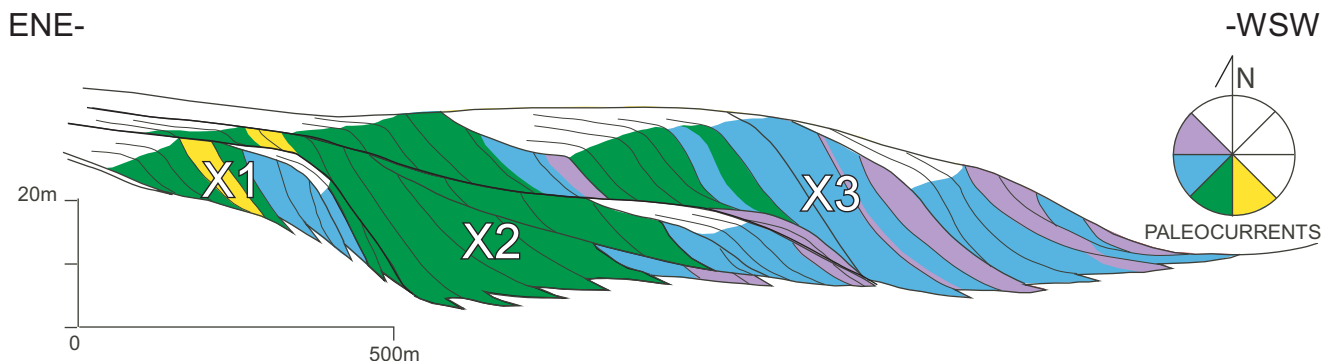


**FIGURE 12** | Outcrop-based cross-section from the correlation of 7 stratigraphic logs representing unit X from the Roda Sandstone (modified from López-Blanco 1996) showing the stratal architecture and paleocurrent distribution within the represented sandwedge. Color scale indicates the paleocurrents measured in the outcrop. Notice the clockwise paleocurrent evolution within each sub-unit (bounded by thick black lines) and in the whole X sandbody.
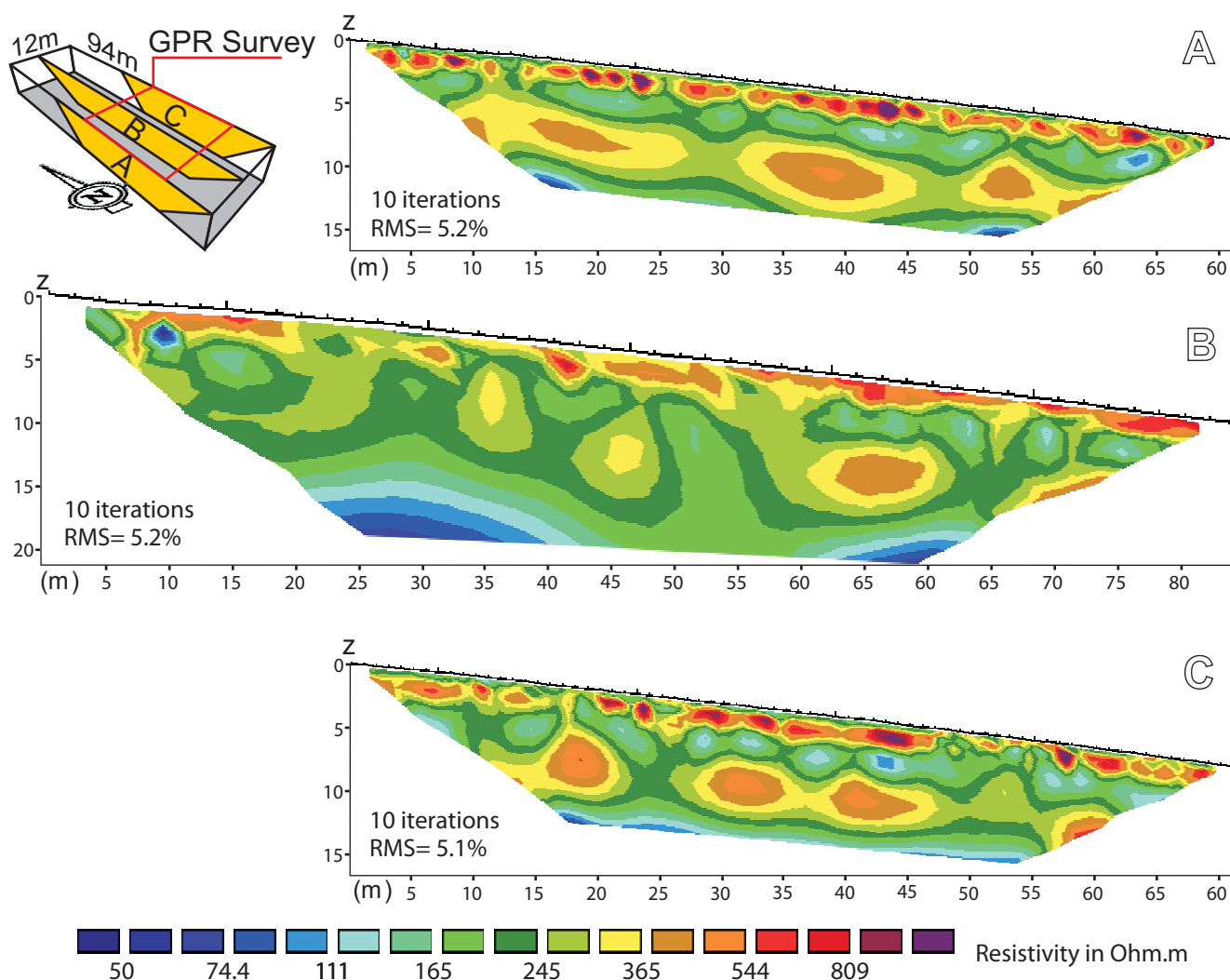
**FIGURE 13** | ERT profiles resulting from the 2D inversion of electrical tomography measurements (their location respecting to GPR data can be seen in Fig. 5). Notice the distribution of values parallel to the top surface.

$Z_4$ sandbody top. Looking at the field data, we know that $Z_4$ thickness in the study area is 10 to 15metres. Thus, the low resistivity unit probably represents the muddy unit just below $Z_4$ (Fig. 2).

## DISCUSSION

One of the most interesting results obtained from the GPR data is the clockwise variation of paleocurrent directions, similar to that observed at larger scales in the same system. The study of the outcrop face beside the GPR cube shows an alternation of sets with different megaforeset facies made up by massive delta front mouthbar sandstones (units A and C) and composite delta front sandstones with oblique megaripple cross-bedding (units B and D) which correlate with the GPR results. This alternation reflects the variation, in a fixed

position, on the balance between south-directed river currents, as an initial supply for the delta front building (mouthbar), and west-directed marine tidal currents, reworking and redistributing sediment in a strike direction. Depending on the balance between those currents, the resulting progradation will be southwards or west-wards-directed.

The clockwise variation of paleocurrents at kilometers to hundred of meters scale was formerly interpreted as related to the funneling of marine (tidal) currents, associated with the paleo-topography created by syn-sedimentary fold growth, during high-frequency relative sea-level falls (López-Blanco, 1996; López-Blanco *et al.*, 2003).

In the GPR studied volume, due to the small scale of the outcrop and observed couplets, the origin of these paleo-
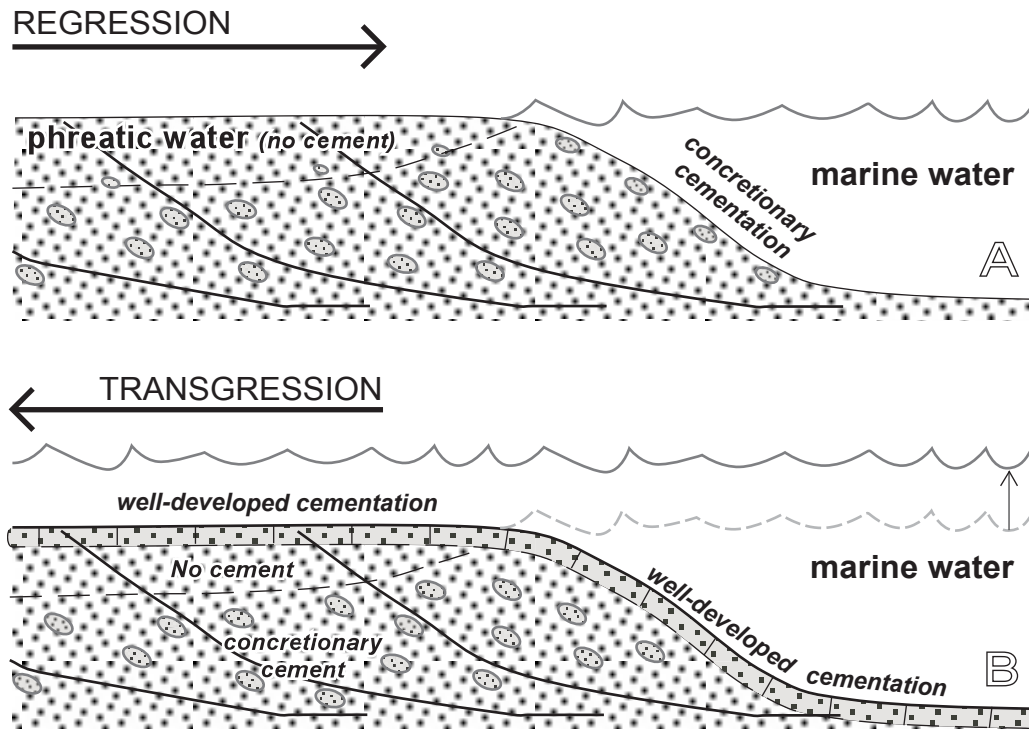
**FIGURE 14** | Sketch showing the origin of the different cementation levels during regressive and transgressive episodes. A) Development of nodular cementation in the sediment-marine water interface, related to short residence-time below the seafloor, and non-cementation or cement dissolution related to phreatic waters during the regressive stage. B) Occurrence of well-developed cementation (hardground) associated with long-term exposure of the sediment to marine water during the transgressive stage.

current variations is not easy to link to a unique and unambiguous controlling factor. The most plausible control is the autocyclic dynamics of a supply-dominated delta front with variations in the fluvial currents (sedimentary flux) resulting in high to low input (and abandonment) cycles. When fluvial sediment supply and currents are strong, massive delta front mouthbar sandstones were deposited in subtidal environments with no significant tidal reworking. If the strength of continental current decreases (eg. channel migration or shifting) tidal currents will be able to rework and redistribute sediments. In this case, the oblique orientation of tidal currents is related to the complex basin configuration due to synsedimentary folding as demonstrated in López-Blanco (1996) and López-Blanco *et al*. (2003). The erosional truncation surface between sets would be produced by tidal currents on an abandoned mouthbar lobe. Thus, the cycles observed in the studied couplets represent the initial mouthbar building from fluvial input currents, the later reworking by transverse tidal currents and a final tidal erosion.

Allocyclic variations, as very-high-frequency relative sea level falls (as in the larger-scale examples) or very-low-frequency tidal cycles, are much more unlikely choices when compared to autocyclic controls. Time constraints (López-Blanco *et al.,* 2003) indicate that the observed cycles are far below precession cyclicity.

Another outstanding result is the vertical cementation zones highlighted by the ERT data. The three different cementation horizons in the sandstone body provide some information about the early diagenetic processes associated with the development of regressive-to-transgressive cycles.

The concretionary calcite cementation on the lower half of the sandbody represents a poorly developed early cementation due to short residence time below the seafloor (Hlal, 2008). This is related to high rates of sediment input during regressive (RST) episodes (Fig. 14) not allowing long residence periods under the sea floor because of the quick burial.

The intermediate poorly cemented horizon, is probably related to the presence of meteoric phreatic water in the uppermost part of the delta front during (or soon after) sandstone deposition, not allowing (or dissolving) early cementation (Fig. 14). Thus, during delta progradation (RST) there is the development of early concretionary (nodular) cementation in deeper parts of the sandy delta front whereas in shallower areas, the influence of phreatic waters led to the dissolution or non precipitation of early cement. The presence of phreatic water reaching previous subtidal deposits was probably enhanced during relative sea-level

falls. These falls (López-Blanco, 1996; Marzo *et al.*, 1998; López-Blanco *et al.*, 2003) led to the final progradation of the regressive systems tract. The uppermost highly cemented horizon represents a hardground caused by the development of an early carbonate cement (aragonite-rich), matrix infiltration and bioturbation (Martinius and Molenaar, 1991) generated during the transgressive event after the end of the delta progradation (Fig. 14). This high grade of cementation is related to a relatively large residence time below the sea water (Hlal, 2008).

## CONCLUSIONS

Most of the subsurface geophysical data show features previously observed in the outcrop. This fact is a positive way to verify GPR as a robust tool for the analogue 3D imaging and reconstruction.

Dip and azimuth analysis of the 3D reflectors by using radar attributes enabled a detailed study of their orientations in the prism, allowing the study of paleocurrent distribution and delta evolution at a scale of megaforeset surfaces. Data attributes allow extracting a statistical representative number of parameters in 3D that would be difficult to obtain from direct field observations (*i.e.* outcrop measurements). In fact, these statistical representative parameters obtained from GPR data are not otherwise available at outcrop scale or from core data. Those parameters can be used in subsequent reservoir modeling.

The internal depositional architecture of the sandbody is characterized by couplets of sandstone sets (radar units), bounded by erosional and/or non-depositional surfaces, arranged with a clockwise variation of the paleocurrents similar to the observed pattern at a greater scale on the Roda Sandstone outcrops. This architectural arrangement is probably related to the autocyclic dynamics of a supply-dominated delta front, with variations in the fluvial currents resulting in high to low input (and abandonment) cycles where fluvial and tidal currents are in competition.

The ERT data show conductivity changes within the sandbody and depict the heterogeneous cementation distribution caused by depositional and early diagenetic processes. These results were constrained with outcrop observations. On the regressive part of transgressive-regressive cycles three main cementation horizons are developed in response to the residence time below marine water related to the development of regressive and transgressive systems tracts. The intermediate non-cemented horizon is related to phreatic water influence, probably enhanced during relative sea-level falls.

The combined analysis between GPR and ERT data provide a complete image of the flow barriers within the sandbody. GPR interpretation depicts the distribution of primary heterogeneities (stratification) and is useful to interpret the internal structure and define depositional units. On the other hand, ERT shows the main electrical conductivity changes of the geologic materials and has been effective to observe the gradual composition changes produced by diagenetic cementation.

## REFERENCES

Annan, A.P., Cosway, S.W., 1994. GPR frequency selection. Kitchener (Ontario, Canada), June 12-16, Proceeding of the Fifth International Conference on Ground Penetrating Radar, 747-760.

Brown, L.F., Fisher, W.L., 1980. Seismic stratigraphy interpretation and petroleum exploration. Tulsa (Oklahoma), Continuing Education Course Note Series 16. American Association of Petroleum Geologists Tulsa, 56pp.

Corbeanu, R.M., Soegaard, K., Szerbiak, R.B., Thurmond, J.B., McMechan, G.A., Wang, D., Snelgrove, S.H., Forster, C.B., Menitove, A., 2001. Detailed internal architecture of a fluvial channel sandstone determined from outcrop, cores and 3-D ground-penetrating radar: example from the mid-Cretaceous Ferron Sandstone, east-central Utah. American Association of Petroleum Geologists Bulletin, 85, 1583-1608.

Corbeanu, R.M., Wizevich, M.C., Bhattacharya, J.P., Zeng, X., McMechan, G.A., 2004. 3-D architecture of ancient lower delta plain point bars using groundpenetrating radar, Cretaceous Ferron Sandstone, Utah. In: Chidsey, T.C., Adams, R.D., Moris, T.M. (eds.). Regional to wellbore analog for fluvial-deltaic reservoir modeling: The Ferron Sandstone of Utah: American Association of Petroleum Geologists, Studies in Geology, 50, 427-449.

Crumeyrolle, P., Soudet, H., López-Blanco, M., Roda Team, 1991. Partitioning of a deltaic reservoir controlled by base-level changes. A case study: the Roda Deltaic Complex. Notingham (United Kingdom), 13th International Sedimentological

Congress, International Association of Sedimentologists (IAS), Abstracts, 114-115.

Davis, J.L., Annan, A.P., 1989. Ground penetrating radar for high resolution mapping of soil and rock stratigraphy. Geophysical Prospecting, 37, 531-551.

Gawthorpe, R.L., Collier, R.E.Ll., Alexander, J., Leeder, M., Bridge, J.S., 1993. Ground penetrating radar: application to sandbody geometry and heterogeneity studies. In: North, C.P., Prosser, D.J. (eds.). Characterisation of Fluvial and Aeolian Reservoirs. Geological Society of London, 73 (Special Publications), 73, 421-432.

Grasmueck, M., Weger, R., Horstmeyer, H., 2005. Full-resolution 3D GPR imaging. Geophysics, 70, K12-K10.

Groenenboom, J., van der Kruk, J., Zeeman, J.H., 2001. 3D GPR data acquisition and the influence of positioning errors on image quality. Amsterdam, 11-15 June 2001, 63rd Conference and Technical Exhibition, 4pp.

Hlal, O., 2008. Diagenesis and Reservoir-Quality Evolution of Paralic, Shallow Marine and Fluvio-lacustrine Deposits. Links to Depositional Facies and Sequence Stratigraphy. Doctoral Thesis. Uppsala Universitet, 66pp.

Jol, H.M., Bristow, C.S., 2003. GPR in sediments: advice on data collection, basic processing and interpretation, a good practice guide. In: Bristow, C.S., Jol, H.M. (eds.). Ground Penetrating Radar in Sediments. Geological Society of London, 211 (Special Publications), 211, 9-27.

Jol, H.M., Bristow, C.S., Smith, D.G., Junck, M.B., Putnam, P., 2003. Stratigraphic imaging of the Navajo Sandstone using ground-penetrating radar. Lead. Edge, 22, 882-887.

Lee, K., Zeng, X.X., McMechan, G.A., Howell, C.D., Bhattacharya, J.P., Marcy, F., Olariu, C., 2005. A ground penetrating radar survey of a delta-front reservoir analog in the Wall Creek Member, Frontier Formation, Wyoming. American Association of Petroleum Geologists Bulletin, 89, 1139-1155.

Lee, K., Gani, M.R., McMechan, G.A., Bhattacharya, J.P., Nyman, S.L., Zeng, X., 2007. Three-dimensional facies architecture and three-dimensional calcite concretion distributions in a tide-influenced delta front, Wall Creek Member, Frontier Formation, Wyoming. American Association of Petroleum Geologists Bulletin, 91, 191-214.

Lee, K., Szerbiak, R., McMechan, G.A., Hwang, N., 2009. A 3-D ground-penetrating radar and wavelet transform analysis of the morphology of shoreface deposits in the Upper Cretaceous Ferron Sandstone Member, Utah. American Association of Petroleum Geologists Bulletin, 93, 181-201.

Lehmann, F., Green, A.G., 2000. Topographic migration: Implications for acquisition and processing. Geophysics, 65, 836-848.

Loke, M.H., Barker, R.D., 1996. Rapid least-squares inversion of apparent resistivity pseudosections by a quasi-Newton method. Geophysical Prospecting, 44, 131-152.

López-Blanco, M., 1996. Estratigrafía secuencial de sistemas deltaicos de cuencas de antepaís: ejemplos de Sant Llorenç del Munt, Montserrat y Roda (Paleógeno, Cuenca de antepaís surpirenaica). Doctoral Thesis. Barcelona (Spain), Universitat

de Barcelona, Acta Geologica Hispanica, 31(4, Abridged version), 91-95.

López-Blanco, M., Marzo, M., Muñoz, J.A., 2003. Low-amplitude, synsedimentary folding of a deltaic complex: Roda Sandstone (Lower Eocene), South-Pyrenean Foreland Basin. Basin Research., 15, 73-96.

Marzo, M., Muñoz, J.A., Vergés, J., López Blanco, M., Roca, E., Arbués, P., Barberà, X., Cabrera, L., Colombo, F., SerraKiel, J., 1998. Sedimentation and tectonics: case studies from Paleogene continental to deep water sequences of the South-Pyrenean Foreland Basin (NE Spain). In: Meléndez-Hevia, A., Soria, A.R. (eds.). Instituto Tecnológico Geo-minero de España, Madrid. 15th International Association of Sedimentologists Field Trip Guide Book, 199-251.

Martinius, A.W., Molenaar, N., 1991. A coral-mollusc (Goniarea-Crassatella) dominated hardground community in a siliciclastic-carbonate sandstone (the Lower Eocene Roda Formation, Southern Pyrenees, Spain). Palaios, 6, 142-155.

Meigs, A.J., 1997. Sequential development of selected Pyrenean thrust faults. Journal of Structural Geology, 19, 481-502.

Mitchum, R.M.Jr., Vail, P.R., Sangree, J.B., 1977a. Seismic stratigraphy and global changes of sea level, Part 6: stratigraphic interpretation of seismic reflection patterns in depositional sequences. In: Payton, C.E. (ed.). Seismic Stratigraphy-applications to hydrocarbon exploration. American Association of Petroleum Geologists Memoir, 117-133.

Mitchum, R.M.Jr, Vail, P.R., Thompson, S.III, 1977b. Seismic stratigraphy and global changes of sea level, Part 2: the depositional sequence as a basic unit for stratigraphic analysis. In: Payton, C.E. (ed.). Seismic Stratigraphy-applications to hydrocarbon exploration, American Association of Petroleum Geologists Memoir, 26, 53-62.

Molenaar, N., Van de Bilt, G.P., Van den Hoeck Ostende, E.R., Nio, S.D., 1988. Early diagenetic alteration of shallow marine mixed sandstones: an example from the Lower Eocene Roda Sandstone Member, Tremp-Graus Basin, Spain. Sedimentary Geology, 55, 295-318.

Muñoz, J.A., 1992. Evolution of a continental collision belt: ECORS-Pyrenees crustal balanced cross-section. In: McClay, K.R. (eds.). Thrust Tectonics. London, Chapman & Hall, 235-246.

Muñoz, J.A., 2002. Alpine tectonics I: the Alpine system north of the Betic Cordillera: the Pyrenees. In: Gibbons, W., Moreno, T. (eds.). London. The Geology of Spain. Geological Society, 370-385.

Nio, S.D., 1976. Marine transgressions as a factor in the formation of sandwave complexes. Geologie en Mijnbouw, 55, 18-40.

Pringle, J.K., Clark, J.D., Westerman, A.R., Gardiner, A.R., 2003. The use of GPR to image three-dimensional (3D) turbidite channel architecture in the Carboniferous Ross Formation, County Clare, western Ireland. In: Bristow, C.S., Jol, H.M. (eds.). Ground Penetrating Radar in Sediments. Geological Society of London, 211 (Special Publications), 315-326.

Puigdefàbregas, C., Samsó, J.M., Serra-Kiel, J., Tosquella, J., 1985. Facies analysis and faunal assemblages of the Roda sandstone formation, Eocene of the southern Pyrenees.

Abstracts 6th Regional Meeting of Sedimentology. Lérida, Spain. International Association of Sedimentologists, 639-642.

Szerbiak, R.B., McMechan, G.A., Corbeanu, R.M., Forster, C., Snalgrove, S.H., 2001. 3-D characterization of a clastic reservoir analog: From3-D GPR to a fluid permability model. Geophysics, 66, 1026-1037.

Tosquella, J., 1988. Estudi Sedimentològic i Biostratigràfic de la Formació Gresos de Roda (Eocè, Conca Tremp-Graus). Msc. Thesis. Barcelona, Universitat de Barcelona, 540pp.

Tingdahl, K.M., 2003. Improving seismic chimney detection using directional attributes. Developments in Petroleum Science, 51, 157-173.

Tinterri, R., 2007. The Lower eocene Roda sandstone (South-central Pyrenees): an example of a flood-dominated river-delta system in a tectonically controlled basin. Rivista italiana di paleontologia e stratigrafia, 113, 223-256.

Ward, S.H., 1990. Resistivity and Induced Polarization Methods. In: Ward, S.H. (ed.). Geotechnical and environmental geophysics. Tulsa, Society of Exploration Geophysicists, 1, 147-189.

Van Eden, J.G., 1970. A reconnaissance of deltaic environment in the Middle Eocene of the south-central Pyrenees, Spain. Geologie en Mijnbouw, 49(2), 145-157.

Yang, C.S., Nio, S.D., 1989. An Ebb-tide depositional model -a comparision between the modern Eastern Scheldt tidal basin (southwest Netherlands) and the Lower Eocene Roda Sandstone in the southern Pyrenees (Spain). Sedimentary Geology, 64, 175-196.